Efficient and Targeted Suppression of Human Lung Tumor Xenografts in Mice with Methotrexate Sodium Encapsulated in All-Function-in-One Chimeric Polymersomes

Weijing Yang, Yan Zou, Fenghua Meng, Jian Zhang, Ru Cheng, Chao Deng, and Zhiyuan Zhong**

The development of virus-mimicking nanoparticles to efficiently load and selectively deliver potent anticancer drugs to the tumor site has received widespread interests.[1] Notably, in contrast to enormous work on lipophilic drugs,[2] significantly less effort has been directed to water soluble small molecule anticancer drugs, partly due to the fact that very few nanosystems can hold hydrophilic chemotherapeutic agents. Liposomes, nanocapsules, and polymersomes containing a large watery core are among the most ideal vehicles for water soluble drugs.[3] They generally show, however, a low drug loading content and efficacy except for doxorubicin hydrochloride (DOX·HCl) that is actively loaded into liposomes and polymersomes via a pH-gradient methodology.[4] As a matter of fact, pegylated liposomal DOX·HCl (Doxil/Caelyx) is the first nanomedicine approved for use in the clinics.[5] In addition to drug loading issue, targeted delivery of water soluble drugs, as for other chemotherapeutics, encounters also challenges of in vivo stability, tumor selectivity, and effective intracellular drug release.[6]

Here, we report on a novel anisamide-functionalized reversibly cross-linked chimeric polymersome (Anis-RCCP) that shows efficient loading and in vivo lung tumor-targeting delivery of a water soluble clinical anticancer drug, methotrexate sodium (MTX·2Na), resulting in complete tumor growth inhibition, 100% survival rate, and depleted adverse effects (**Figure 1**a). MTX·2Na (Trexall) is prescribed and used for the treatment of rheumatoid arthritis, severe psoriasis, and various types of cancers including breast, leukemia, lymphoma, lung, and osteosarcoma. MTX·2Na takes effects by prohibiting the metabolism of folic acid via competitively inhibiting dihydrofolate reductase, an enzyme participating in the tetrahydrofolate synthesis. MTX·2Na suffers, nevertheless, a poor pharmacokinetics and narrow therapeutic window, which significantly limits its therapeutic outcomes.[7] In the past years, different delivery approaches such as MTX-polymer conjugates[8] and MTX-encapsulated liposomes, micelles, and nanoparticles[9] have been explored to reduce its dose-limiting side effects and increase therapeutic efficacy. However, none of these systems have advanced to the clinical settings due to problems of complex fabrication, low drug loading, fast drug leakage, or poor tumor selectivity.[10] Here, Anis-RCCP was formed from poly(ethylene glycol)-*b*-poly(N-2-hydroxypropyl methacrylamide-*g*-lipoic acid)-*b*-poly(2-(dimethylamino)ethyl methacrylate) (PEG-P(HPMA-LA)-PDMA) and Anis-PEG-P(HPMA-LA)-PDMA asymmetric triblock copolymers, in which PEG was longer than PDMA. The presence of positively charged PDMA in the watery core would allow efficient loading of MTX·2Na. The vesicular membrane is made of P(HPMA-LA), which can be readily cross-linked in the presence of catalytic dithiothreitol (DTT) to stabilize polymersomes and prevent drug leakage. Under cytoplasmic reductive conditions, nevertheless, the polymersomes would be automatically decrosslinked, leading to fast intracellular drug release. PHPMA is a biocompatible and water soluble polymer widely investigated for drug delivery.[11] LA is a natural antioxidant produced by the human body and used to treat diabetic neuropathy.[12] The decoration of polymersome surface with anisamide would impart high affinity and targetability to sigma receptors that are overexpressed on many human malignancies including lung cancers.[13] Lung cancer has become a leading cause of death worldwide.

PEG-P(HPMA-LA)-PDMA and Anis-PEG-P(HPMA-LA)-PDMA triblock copolymers were synthesized via sequential reversible addition-fragmentation chain transfer (RAFT) polymerization of N-2-hydroxypropyl methacrylamide (HPMA) and 2-(dimethylamino)ethyl methacrylate (DMA) using MeO-PEG-CPADN (CPADN: 4-cyanopentanoic acid dithionaphthalenoate, $M_{n,PEG}$ = 5.0 kg mol^{-1}) and Anis-PEG-CPADN ($M_{n,PEG}$ = 7.5 kg mol^{-1}) as a macro-RAFT agent, respectively, followed by lipoylation (Scheme S1, Supporting Information). CPADN is a robust and versatile RAFT agent with which we have previously prepared a series of well-defined block copolymers such as PEG-PCL-PDEA and PEG-PTTMA-PAA.[14]^{1}H NMR of PEG-PHPMA-PDMA clearly displayed signals attributable to PHPMA (δ 0.8-1.03, 2.89, 3.67, and 4.71), PDMA (δ 1.3-1.8, 2.27, 2.53, 4.18), and PEG (δ 3.23 and 3.51) (Figure S1a, Supporting Information). The M_n of PEG-PHPMA-PDMA was determined to be 5.0-11.8-1.8 kg mol^{-1} by

W. Yang, Dr. Y. Zou, Prof. F. Meng, Dr. J. Zhang, Dr. R. Cheng, Prof. C. Deng, Prof. Z. Zhong
Biomedical Polymers Laboratory
and Jiangsu Key Laboratory of Advanced Functional Polymer Design and Application
College of Chemistry
Chemical Engineering and Materials Science
Soochow University
Suzhou 215123, P. R. China
E-mail: fhmeng@suda.edu.cn; zyzhong@suda.edu.cn

DOI: 10.1002/adma.201600065

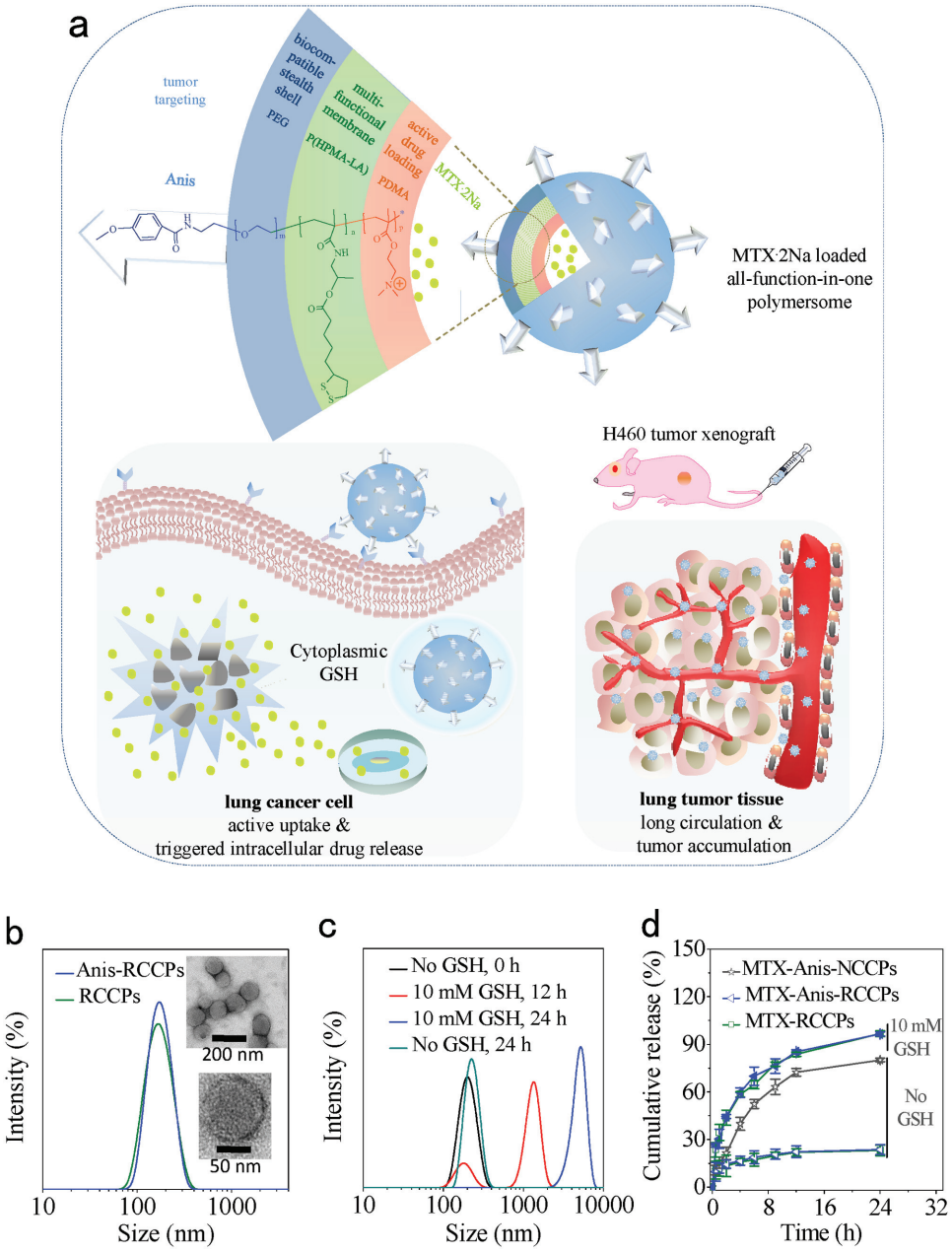

Figure 1. Schematic illustration and characterizations of Anis-RCCPs. a) Structure and functions of Anis-RCCPs in targeted delivery of MTX·2Na to H460 human lung tumor-bearing nude mice, b) the size and size distribution measured by DLS (Inset: TEM image of Anis-RCCPs stained with phosphotungstic acid), c) size change of Anis-RCCPs in response to 10×10^{-3} M GSH, and d) the in vitro MTX·2Na release in PB at pH 7.4 and 37 °C. The polymersome concentration was set at 100 μg mL^{-1} ($n = 3$).

comparing the integrals of signals at δ 3.67 (methine proton next to the hydroxyl group in PHPMA) and 2.27 (methylene protons neighboring to the nitrogen atom in PDMA) to 3.51 (methylene protons of PEG). Gel permeation chromatography (GPC) showed that the copolymer after trifluoroacetation had a unimodal distribution with a low M_w/M_n of 1.15 and an M_n of 16.0 kg mol^{-1} (Table S1, Supporting Information), close to that calculated from ^{1}H NMR. ^{1}H NMR of Anis-PEG-PHPMA-PDMA displayed besides signals attributable to PEG-PHPMA-PDMA also aromatic protons of anisamide at δ 6.97 and 7.83 (Figure S2a, Supporting Information). In a similar way, Anis-PEG-PHPMA-PDMA was determined to have an M_n of 7.5-12.0-2.3 kg mol^{-1} (^{1}H NMR) and an M_w/M_n of 1.21 (GPC).

The treatment of PEG-PHPMA-PDMA and Anis-PEG-PHPMA-PDMA with lipoic acid anhydride (LAA) in DMSO at a hydroxyl/LAA mole ratio of 1/1 yielded PEG-P(HPMA-LA)-PDMA (Figure S1b, Supporting Information) and Anis-PEG-P(HPMA-LA)-PDMA (Figure S2b, Supporting Information). ^{1}H NMR showed besides signals attributable to PHPMA, PDMA, and PEG, also resonances of lipoyl ester moieties at δ 1.40,

1.58-1.69,1.89/2.43, 2.29, 3.02, and 3.74. In addition, signals at δ 4.71 owing to the hydroxyl group of PHPMA diminished following lipoylation while a new signal due to the methine proton next to the ester bond appeared at δ 4.83. The comparison of the integrals of signals at δ 1.40 (γ-methylene protons of LA moieties) and 3.51 (PEG methylene protons) indicated that both copolymers had nearly quantitative LA substitution (Table S1, Supporting Information).

Anis-RCCPs were prepared from co-self-assembly of PEG-P(HPMA-LA)-PDMA and Anis-PEG-P(HPMA-LA)-PDMA at 1/1 weight ratio followed by autocrosslinking in the presence of DTT. Dynamic light scattering (DLS) measurements showed that Anis-RCCPs had a unimodal size distribution with an average size of ≈174 nm (Figure 1b) and slightly postive zeta potential (Table S2, Supporting Information). Transmission electron microscopy (TEM) image confirmed that Anis-RCCPs had a vesicular structure and spherical morphology. UV spectra clearly showed absence of characteristic absorbance of dithiolane ring at 310 nm, in line with formation of linear polydisulfide cross-links in Anis-RCCPs (Figure S3e, Supporting Information). Anis-RCCPs displayed excellent colloidal stability against extensive dilution, high salt condition, and cell culture media (Figure S3, Supporting Information), while quickly destabilized and formed large aggregates of 1400 nm in 12 h and over 5000 nm in 24 h in response to 10×10^{-3} M glutathione (GSH) at pH 7.4 and 37 °C (Figure 1 c). In sharp contrast, the noncrosslinked polymersomes (Anis-NCCPs) exhibited poor colloidal stability against high salt condition and cell culture media under otherwise the same conditions. The fast swelling and aggregation of Anis-RCCPs in response to GSH is due to the fact that reductive decrosslinking transforms the lipoyl group into more hydrophilic dihydrolipoyl group, significantly increasing the hydrophilicity of the vesicular membranes. Similar phenomena were also observed for disulfide-crosslinked nanoparticles.[15] RCCPs formed from PEG-P(HPMA-LA)-PDMA alone had a similar size distribution and were used as a nontargeting control.

As expected, Anis-RCCPs and RCCPs could efficiently load MTX·2Na. At a theoretical drug loading content (DLC) of 30 wt%, a loading efficiency of 65.1%, which corresponded to a high DLC of 22.0 wt%, was obtained. Notably, MTX·2Na-loaded Anis-RCCPs (MTX-Anis-RCCPs) had an average size of 147 nm (Table S2, Supporting Information), which was ≈30 nm smaller than blank Anis-RCCPs, likely resulting from the strong interaction between MTX and PDMA chains in the lumen. MTX·2Na-loaded RCCPs (MTX-RCCPs) had a close to neutral zeta potential, supporting a chimeric vesicular structure with PEG preferentially located at the outer surface and PDMA at the inner surface. The in vitro release studies showed that MTX release from Anis-RCCPs and RCCPs was minimal (<20 % in 24 h) at physiological conditions (pH 7.4 and 37 °C) whereas nearly quantitative release was observed in the presence of 10×10^{-3} M GSH under otherwise the same conditions (Figure 1d). Notably, MTX-Anis-RCCPs under a reductive condition showed even faster drug release than the noncrosslinked counterparts (MTX-Anis-NCCPs) under a nonreductive condition. This ultrafast redox-responsive drug release of MTX-Anis-RCCPs is due to increased hydrophilicity of the polymersomal membrane and swelling of the polymersomes, both leading to significantly enhanced drug diffusion.

3-(4,5-Dimethylthiazol-2-yl)-2,5-diphenyltetrazoliumbromide (MTT) assays revealed that blank Anis-RCCPs and RCCPs were practically nontoxic to sigma receptor overexpressing H460 cells at tested concentrations ranging from 0.1 to 0.5 mg mL^{-1} (**Figure 2**a), confirming that they possess excellent biocompatibility. MTX-Anis-RCCPs showed a high potency against H460 cells with a low half-maximal inhibitory concentration (IC_{50}) of 2.4 μg mL^{-1} (4.81×10^{-6} M), which was ≈4 and tenfold lower than that of MTX-RCCPs (nontargeted control) and free MTX·2Na, respectively (Figure 2b). The systemic studies on Anis-RCCPs with varying Anis contents revealed that 50% Anis gave the best targetability to H460 cells (Figure S4, Supporting Information). The competitive inhibition experiments showed that pretreating H460 cells with haloperidol (an antagonist to block the sigma receptors) resulted in fivefold increase of IC_{50} for MTX-Anis-RCCPs, confirming that Anis-RCCPs were taken up by H460 cells via a sigma receptor mediated endocytosis mechanism.

The cellular uptake and intracellular drug release behaviors of MTX-Anis-RCCPs in H460 cells were investigated using fluorescein isothiocyanate (FITC)-labeled MTX·2Na (FITC-MTX) by flow cytometry and confocal laser scanning microscope (CLSM). The flow cytometric studies demonstrated that FITC-MTX level in H460 cells treated with FITC-MTX-Anis-RCCPs was ≈7.5 and 3.3-fold higher than those with free FITC-MTX and FITC-MTX-RCCPs, respectively (Figure 2c). The pretreatment of H460 cells with haloperidol prior to incubation with FITC-MTX-RCCPs resulted in significantly reduced FITC-MTX level, in good agreement with MTT results. Interestingly, CLSM observed strong FITC fluorescence throughout the whole H460 cells including the cell nuclei after 4 h incubation with FITC-MTX-Anis-RCCPs (Figure 2d). In contrast, FITC fluorescence in H460 cells treated with FITC-MTX-RCCPs (nontargeting control) was much weaker, and negligible FITC fluorescence was observed in free FITC-MTX treated cells. These results confirmed fast and efficient uptake of Anis-RCCPs by H460 cells via sigma receptor mediated endocytosis and quick intracellular release of FITC-MTX.

The intracellular trafficking of FITC-MTX-Anis-RCCPs was further studied at varying incubation times from 0.5, 1, 2, to 4 h. The endosomes were stained with Lysoltracker-red. Intriguingly, the results showed that FITC-MTX has been delivered and released into H460 cells in 0.5 h and to the nuclei of H460 cells in 1 h (Figure 2e). Notably, while a significant amount of drug remains entrapped in the endosomes in 1 h, most FITC-MTX has escaped from endosomes in 2 h and strong FITC-MTX fluorescence is observed throughout the whole cell. The fast cytoplasmic and nucleic delivery of FITC-MTX by Anis-RCCPs could be due to their effective endosomal escape following receptor-mediated endocytosis, resulting from the proton sponge effect of PDMA.[15a] Another possible reason is that FITC-MTX-Anis-RCCPs are also partly internalized by H460 cells through a different mechanism from endocytosis.

For in vivo studies, we used clinical MTX·2Na injection (Trexall) as a control. The in vivo pharmacokinetics studies in mice showed that both MTX-Anis-RCCPs and MTX-RCCPs had a significantly longer circulation time than Trexall (**Figure 3**a). The elimination half-life ($t_{1/2,\beta}$) was 5.24 and 4.32 h for MTX-Anis-RCCPs and MTX-RCCPs, respectively. In comparison,

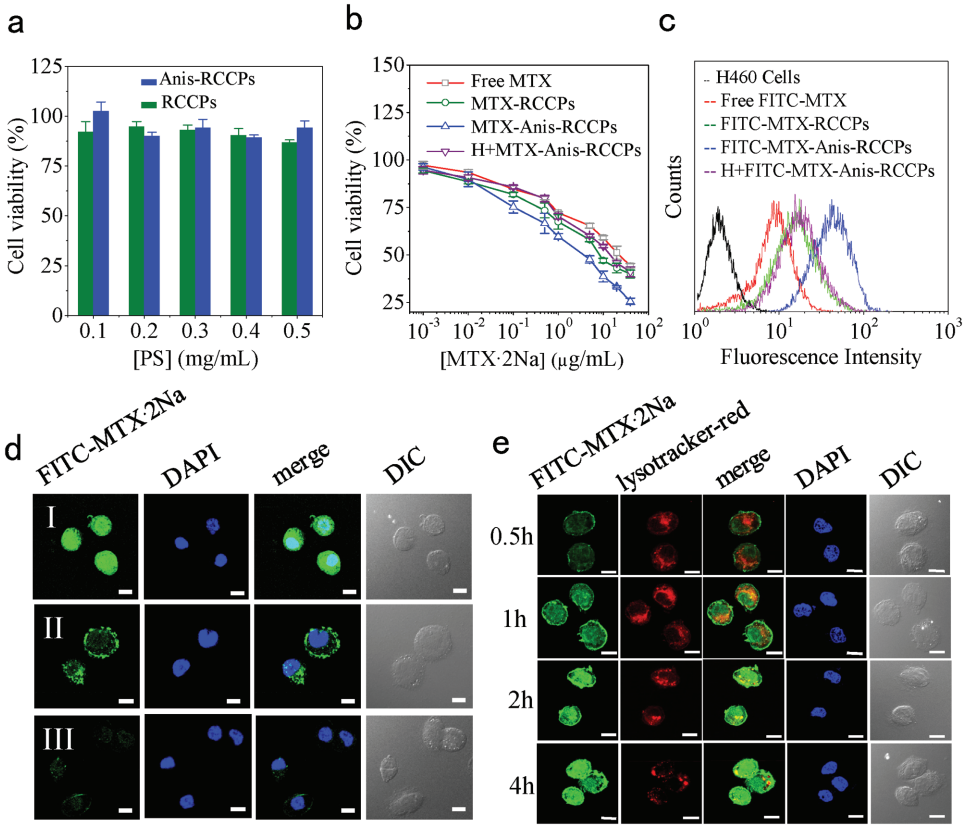

Figure 2. The in vitro cell experiments. a) MTT assays of H460 cells following 48 h incubation with empty Anis-RCCPs and RCCPs. b) The concentration-dependent cytotoxicity of MTX-Anis-RCCPs, MTX-RCCPs, and free MTX·2Na to H460 cells determined using MTT assays. The cells were incubated with different drug formulations for 4 h, the medium was aspirated and replenished with fresh culture medium, and the cells were further cultured for 44 h. The competitive inhibition experiments were carried out by pretreating H460 cells with 30×10^{-6} M haloperidol (H) prior to adding MTX-Anis-RCCPs. Data are presented as the average ± standard deviation ($n = 4$). c) Flow cytometric analysis of FITC levels in H460 cells. H460 cells pretreated with haloperidol and blank H460 cells were used as controls. FITC-MTX dosage was 10 μg mL^{-1}. d) CLSM images of H460 cells following 4 h incubation with FITC-MTX-Anis-RCCPs (I), FITC-MTX-RCCPs (II), and FITC-MTX (III). e) CLSM images of H460 cells at 0.5, 1, 2 or 4 h incubation with FITC-MTX-Anis-RCCPs at a dosage of 10 μg mL^{-1}. The scale bars represent 15 μm.

Trexall had a short $t_{1/2,\beta}$ of 0.29 h. The area under the curve for MTX-Anis-RCCPs and MTX-RCCPs were 133.2 and 119.3 μgh mL^{-1}, which were about 20 times higher than that of free MTX.

The biodistribution of MTX in H460 tumor xenografted mice at 8 h postinjection demonstrated that the mice treated with MTX-Anis-RCCPs had a remarkable MTX tumor accumulation of 5.3% ID g^{-1} (injected dose per gram of tissue), which was about 4.5 and ninefold higher than that with MTX-RCCPs and Trexall, respectively (Figure 3b). It should further be noted that the tumor accumulation of MTX-Anis-CLPs was also significantly higher than in the healthy organs such as heart, spleen, lung, and kidney, except for liver. The calculation of tumor-to-normal tissue (T/N) ratios showed that MTX-Anis-RCCPs exhibited 9.6–25.0 and 3.1–7.8 times higher T/N ratios than Trexall and MTX-RCCPs, respectively (Table S3, Supporting Information). The enhanced tumor selectivity and accumulation of MTX-Anis-RCCPs renders them particularly interesting in the treatment of lung cancers.

The therapeutic performance of MTX-Anis-RCCPs was studied in H460 tumor-bearing nude mice. The mice were injected every three days via the tail vein at a drug dosage of 15 mg MTX equiv. kg^{-1}. MTX-RCCPs, Trexall, and phosphate buffered saline (PBS) were used as controls. Interestingly, the results displayed that MTX-Anis-RCCPs completely suppressed tumor growth (Figure 3c). MTX-RCCPs though less effective than MTX-Anis-RCCPs demonstrated significantly better tumor growth inhibition than Trexall. The photograph of tumor blocks of mice isolated on day 21 confirmed the best inhibition of tumor growth by MTX-Anis-RCCPs. Notably, no body weight loss was observed for mice treated with either MTX-Anis-RCCPs or MTX-RCCPs (Figure 3d), indicating that these polymersomal MTX formulations have little adverse effects. In sharp contrast, significant body weight loss (up to 23%) was discerned for free MTX treated mice.

Remarkably, Kaplan–Meier survival curves showed a 100% survival rate for mice treated with MTX-Anis-RCCPs over an experiment period of 45 d (Figure 3e). In comparison, mice treated with Trexall and MTX-RCCPs all died in 31 and 38 d, respectively. The histological analyses using H&E staining revealed that MTX-Anis-RCCPs caused widespread apoptosis and necrosis of tumor cells while little damage to the liver, kidney, heart, spleen, and lung (Figure 3f; Figure S5, Supporting Information). In spite of significant accumulation of

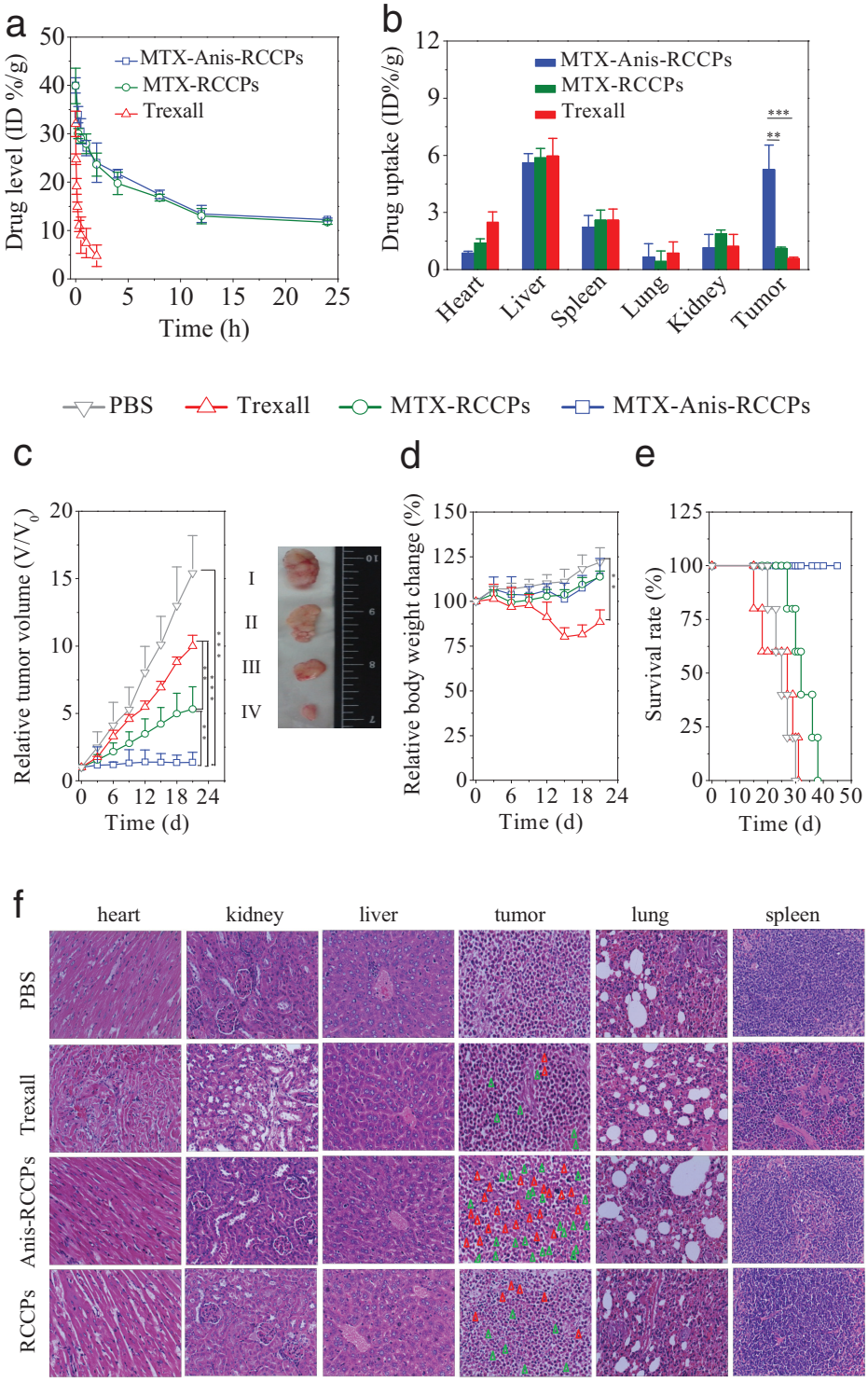

Figure 3. The in vivo pharmacokinetics and antitumor performance of MTX-Anis-RCCPs. a) Blood circulation in nude mice. MTX levels were determined by high performance liquid chromatography (HPLC), and expressed as injected dose per gram of tissue (% ID g^{-1}) ($n = 3$). b) In vivo biodistribution in H460 tumor-bearing nude mice at 8 h post i.v. injection (dosage: 15 mg MTX equiv. kg^{-1}). c) H460 tumor growth inhibition by MTX-Anis-RCCPs. The drug was given on day 0, 3, 6, 9, and 12 at 15 mg MTX equiv. kg^{-1}. The inset shows the photographs of tumor blocks excised on day 21 from mice treated with PBS (I), Trexall (II), MTX-RCCPs (III), and MTX-Anis-RCCPs (IV), respectively. d) Body weight changes of mice following different treatments. e) Survival rates of mice following different treatments within 45 d. Data are presented as mean ± SD ($n = 5$). f) The histological analyses of H&E stained sections of tumor and major organs excised from H460 tumor-bearing nude mice on day 21. The green and red arrows point to apoptotic and necrotic cells, respectively. MTX-RCCPs, Trexall, and PBS were used as controls. (Student's t test, $^{**}p < 0.01$, $^{***}p < 0.001$). The images of tumor and major organs were obtained by a Leica microscope at magnification (400×).

MTX-RCCPs in the liver as observed by biodistribution studies, liver damage was insignificant, likely due to poor uptake by liver cells. In contrast, mice treated with Trexall induced little tumor necrosis but significant damage of heart, kidney, and spleen tissues. It is evident, therefore, that MTX-Anis-RCCPs have superior targetability and therapeutic efficacy in sigma receptor overexpressing H460 tumor xenografts.

In conclusion, we have demonstrated that anisamide-functionalized disulfide-crosslinked chimeric polymersomes can efficiently load and selectively deliver and release MTX·2Na into sigma receptor overexpressing H460 non-small lung cancer cell xenografts in vivo, leading to markedly improved tumor growth inhibition and survival rate as compared to the nontargeting polymersomes and commercial Trexall controls. To the best of our knowledge, this represents the first report on efficient tumor-targeting delivery of MTX·2Na using polymersomes. These disulfide-crosslinked chimeric polymersomes possess several extraordinary features over previously reported nanosystems including high MTX·2Na loading, superior in vivo stability, enhanced accumulation in tumors, selective and efficient uptake by tumor cells, fast intracellular release of MTX·2Na and low side effects, which render them an "all-function-in-one" nanoplatform for safe and potent cancer chemotherapy.

Supporting Information

Supporting Information is available from the Wiley Online Library or from the author.

Acknowledgements

This work was financially supported by research grants from the National Natural Science Foundation of China (NSFC 51273139, 51473111, and 51561135010), the National Science Fund for Distinguished Young Scholars (NSFC 51225302), the major project of Jiangsu Province University Natural Science (14KJA150008), Ph.D. Programs Foundation of Ministry of Education of China (20133201110005), the Jiangsu Higher Education Excellent Science and Technology Innovation Team Program, and a Project Funded by the Priority Academic Program Development (PAPD) of Jiangsu Higher Education Institutions. All animal experiments were approved by the Animal Care and Use Committee of Soochow University (P. R. China), and all protocols of animal studies conformed to the Guide for the Care and Use of Laboratory Animals.

Received: January 6, 2016
Revised: June 11, 2016
Published online: July 6, 2016

[1] a) R. K. Jain, T. Stylianopoulos, *Nat. Rev. Clin. Oncol.* **2010**, *7*, 653; b) D. Peer, J. M. Karp, S. Hong, O. C. FaroKhzad, R. Margalit, R. Langer, *Nat. Nanotechnol.* **2007**, *2*, 751; c) S. Mura, J. Nicolas, P. Couvreur, *Nat. Mater.* **2013**, *12*, 991; d) M. E. Davis, Z. Chen, D. M. Shin, *Nat. Rev. Drug Discov.* **2008**, *7*, 771.

[2] a) R. Dong, Y. Zhou, X. Huang, X. Zhu, Y. Lu, J. Shen, *Adv. Mater.* **2015**, *27*, 498; b) G. K. Such, Y. Yan, A. P. R. Johnston, S. T. Gunawan, F. Caruso, *Adv. Mater.* **2015**, *27*, 2278; c) Y. Zhao, F. Sakai, L. Su, Y. Liu, K. Wei, G. Chen, M. Jiang, *Adv. Mater.* **2013**, *25*, 5215.

[3] a) M. Zhao, B. Hu, Z. Gu, K.-I. Joo, P. Wang, Y. Tang, *Nano Today* **2013**, *8*, 11; b) S. F. M. van Dongen, H. P. M. de Hoog, R. Peters, M. Nallani, R. J. M. Nolte, J. C. M. van Hest, *Chem. Rev.* **2009**, *109*, 6212; c) N. S. Oltra, P. Nair, D. E. Discher, *Annu. Rev. Chem. Biomol.* **2014**, *5*, 281; d) P. Tanner, P. Baumann, R. Enea, O. Onaca, C. Palivan, W. Meier, *Acc. Chem. Res.* **2011**, *44*, 1039; e) H. Cabral, N. Nishiyama, K. Kataoka, *Acc. Chem. Res.* **2011**, *44*, 999; f) K. T. Kim, J. Cornelissen, R. J. M. Nolte, J. C. M. van Hest, *Adv. Mater.* **2009**, *21*, 2787; g) L. Pourtau, H. Oliveira, J. Thevenot, Y. Wan, A. R. Brisson, O. Sandre, S. Miraux, E. Thiaudiere, S. Lecommandoux, *Adv. Healthcare Mater.* **2013**, *2*, 1420.

[4] F. Ahmed, R. I. Pakunlu, A. Brannan, F. Bates, T. Minko, D. E. Discher, *J. Controlled Release* **2006**, *116*, 150.

[5] a) N. Bertrand, J. Wu, X. Xu, N. Kamaly, O. C. Farokhzad, *Adv. Drug Delivery Rev.* **2014**, *66*, 2; b) A. G. Kohli, S. Kivimaee, M. R. Tiffany, F. C. Szoka, *J. Controlled Release* **2014**, *191*, 105; c) Y. Barenholz, *J. Controlled Release* **2012**, *160*, 117.

[6] a) R. Cheng, F. H. Meng, C. Deng, Z. Y. Zhong, *Nano Today* **2015**, *10*, 656; b) C. M. Dawidczyk, C. Kim, J. H. Park, L. M. Russell, K. H. Lee, M. G. Pomper, P. C. Searson, *J. Controlled Release* **2014**, *187*, 133.

[7] Z. A. Khan, R. Tripathi, B. Mishra, *Expert Opin. Drug Delivery* **2012**, *9*, 151.

[8] a) L. M. Kaminskas, V. M. McLeod, D. B. Ascher, G. M. Ryan, S. Jones, J. M. Haynes, N. L. Trevaskis, L. J. Chan, E. K. Sloan, B. A. Finnin, M. Williamson, T. Velkov, E. D. Williams, B. D. Kelly, D. J. Owen, C. J. H. Porter, *Mol. Pharm.* **2015**, *12*, 432; b) A. Jain, A. Jain, N. K. Garg, R. K. Tyagi, B. Singh, O. P. Katare, T. J. Webster, V. Soni, *Acta Biomater.* **2015**, *24*, 140; c) Y. Wang, H. Chen, Y. Liu, J. Wu, P. Zhou, Y. Wang, R. Li, X. Yang, N. Zhang, *Biomaterials* **2013**, *34*, 7181.

[9] a) M. Curcio, B. Blanco-Fernandez, L. Diaz-Gomez, A. Concheiro, C. Alvarez-Lorenzo, *Bioconjugate Chem.* **2015**, *26*, 1900; b) Y. Li, J. Lin, H. Wu, Y. Chang, C. Yuan, C. Liu, S. Wang, Z. Hou, L. Dai, *Mol. Pharm.* **2015**, *12*, 769; c) X. Zhang, Y. Zheng, Z. Wang, S. Huang, Y. Chen, W. Jiang, H. Zhang, M. Ding, Q. Li, X. Xiao, X. Luo, Z. Wang, H. Qi, *Biomaterials* **2014**, *35*, 5148.

[10] S. S. Abolmaali, A. M. Tamaddon, R. Dinarvand, *Cancer Chemother. Pharmacol.* **2013**, *71*, 1115.

[11] Y.-L. Li, L. Zhu, Z. Z. Liu, R. Cheng, F. H. Meng, J.-H. Cui, S.-J. Ji, Z. Y. Zhong, *Angew. Chem. Int. Ed.* **2009**, *48*, 9914.

[12] a) J. Kopecek, P. Kopeckova, *Adv. Drug Delivery Rev.* **2010**, *62*, 122; b) R. Zhang, J. Yang, T.-W. Chu, J. M. Hartley, J. Kopecek, *Adv. Healthcare Mater.* **2015**, *4*, 1054.

[13] a) A. Maczurek, K. Hager, M. Kenklies, M. Sharman, R. Martins, J. Engel, D. A. Carlson, G. Muench, *Adv. Drug Delivery Rev.* **2008**, *60*, 1463; b) S. Park, U. Karunakaran, N. H. Jeoung, J.-H. Jeon, I.-K. Lee, *Curr. Med. Chem.* **2014**, *21*, 3636.

[14] a) J. Della Rocca, R. C. Huxford, E. Comstock-Duggan, W. B. Lin, *Angew. Chem. Int. Ed.* **2011**, *123*, 10514; b) S. K. Kim, M. B. Foote, L. Huang, *Biomaterials* **2012**, *33*, 3959.

[15] a) G. J. Liu, S. B. Ma, S. K. Li, R. Cheng, F. H. Meng, H. Y. Liu, Z. Y. Zhong, *Biomaterials* **2010**, *31*, 7575; b) L. Lu, Y. Zou, W. J. Yang, F. H. Meng, C. Deng, R. Cheng, Z. Y. Zhong, *Biomacromolecules* **2015**, *16*, 1726.

[16] a) J. Li, X. Yu, Y. Wang, Y. Yuan, H. Xiao, D. Cheng, X. Shuai, *Adv. Mater.* **2014**, *26*, 8217; b) Y. N. Zhong, J. Zhang, R. Cheng, C. Deng, F. H. Meng, F. Xie, Z. Y. Zhong, *J. Controlled Release* **2015**, *205*, 144.